Application of an enhanced discrete element method to oil and gas drilling processes

Pere Andreu Ubach · Ferran Arrufat · Lev Ring · Raju Gandikota · Francisco Zárate · Eugenio Oñate

Received: date / Accepted: date

Abstract The authors present results on the use of the discrete element method (DEM) for the simulation of drilling processes typical in the oil and gas exploration industry. The numerical method uses advanced DEM techniques using a local definition of the DEM parameters and combined FEM-DEM procedures.

This paper presents a step by step procedure to build a DEM model for analysis of the soil region coupled to a FEM model for discretizing the drilling tool that reproduces the drilling mechanics of a particular drill bit. A parameter study has been performed to determine the model parameters in order to maintain accurate solutions with reduced computational cost.

Keywords Drilling · Discrete Element Method, Oil and Gas

1 Introduction

This paper presents results obtained in a research effort aimed at evaluating the feasibility of using the discrete element method (DEM) and a combination of the DEM and the finite element method (FEM) for solving real problems and gaining valuable insight in the field of oil and gas drilling engineering. The oil drilling industry, for instance, faces great challenges as the traditional reservoirs become depleted and the companies explore deeper in the Earth crust and further offshore. At greater depths, the drilling conditions are harsher for the material, but also require a more efficient use of the techniques mastered by the drilling companies.

Another consequence of drilling ever deeper holes is the increased cost of the investment for drilling the well. The drilling process takes longer and therefore the associated cost rises and the financial risk increases. Catastrophic failures of the material or the well itself could become prohibitive for the oil companies. Therefore, the smart and efficient use of the engineering and scientific knowledge of all the processes involved is even more critical.

The mechanics of the interaction of the drill bit with the geological formation are one of the aspects about which the industry has traditionally relied on semi-empirical data for conducting its operations. But as the companies explore new boundaries for their wells, that semi-empirical data becomes outranged. Therefore,

P.-A. Ubach, F. Arrufat, F. Zárate, E. Oñate
CIMNE - Centre Internacional de Metodes Numerics en Enginyeria
Campus Norte UPC, 08034 Barcelona, Spain
Tel.: +34-93-2057016
Fax: +34-93-4016517
E-mail: ubach,farrufat,zarate,onate@cimne.upc.edu

L. Ring
Weatherford International
E-mail: Lev.Ring@weatherford.com

R. Gandikota
MindMesh Inc. E-mail: rga@mindmeshinc.com

an important effort in generating advanced models able to reproduce every aspect of the behavior of drill bits is required.

In this paper we study different factors which are relevant for the applications of the DEM to model the mechanics of oil and gas drilling processes. In particular, we study the sensibility of the drill bit mechanics to the damping factor, the rotational speed and the time step factor. The study is performed by simply evaluating the effect of using different values of these parameters in the overall efficiency of the drilling process. An assessment of the optimal particle size has also been performed.

The drilling tools are modelled in three dimensions (3D) with the finite element method (FEM) using 4-noded tetrahedra, while the underlying soil is modelled with the DEM using spherical particles. An adequate contact method is used to account for the interaction of DEM particles and the triangular element mesh discretizing the surface of the drill.

The discrete element method has been tried in the past to address the analysis of drilling operations in the oil industry. A number of issues have prevented the use of DEM in these applications. Computational cost has always been a constant, and although the oil industry is not short on ressources, in many occasions the technology simply was not there. This paper addresses this issue by explaining a methodology for successfully preparing a simulation of a drilling operation. Another important issue in the past was the accuracy of the results. DEM has long been viewed as a very promising computational method for its ability to handle in a natural manner the breaking of the continuum. However, because of the very same nature of the method, it has lagged in its ability to accurately represent the continuum. The authors have already presented improvements on the DEM and demonstrated good accuracy results for the multifracture analysis of geomaterials and concrete [14].

The final goal of this work is to show that the DEM and the combined FEM-DEM techniques described can provide valuable results for laboratory and field engineering in the oil/gas drilling industry.

The layout of the paper is as follows. Section 2 provides a general overview of the DEM. In Sections 3 and 4 the procedure for the construction of the computational model and sensibility of analysis of the drill bit mechanics are presented. This can be understood as general guidelines for creating practical DEM models useful for the oil and gas drilling industry. The paper ends with the conclusions in Section 5.

2 Background on the DEM

The DEM is an effective and powerful numerical technique for reproducing multifracture and failure of granular and cohesive geomaterials (soils, rocks, concrete), masonry and ceramic material, among others. In the DEM it is typically assumed that the underlying material (either of granular or cohesive type) can be represented as a collection of rigid particles (spheres or balls in 3D and discs in 2D) interacting among themselves in the normal and tangential directions at the contact interfaces between adjacent particles.

The particular features of a DEM model depend basically on the constitutive expression for the normal and shear stiffness parameters at the contact interface, the frictional coefficient, the damping parameter and the failure conditions at the interface.

Two different approaches can be followed for determining the DEM constitutive parameters for a cohesive material, namely the global approach and the local approach. In the global approach *uniform global* DEM properties are assumed in the whole discrete element assembly. The values of the global DEM parameters can be found using different procedures. Some authors [4, 6, 7] have used numerical experiments for determining the relationships between DEM and continuum parameters expressed in dimensionless form. This method has been used by the authors in previous works [9–12, 17–20]. Other procedures for defining the global DEM parameters are based on the definition of average particle size measures for the whole discrete particle assembly and then relating the global DEM and continuum parameters via laboratory tests.

A second approach used in this work, is to assume that the DEM parameters depend on the *local properties* of the interaction particles, namely their radii and the continuum parameters at each interaction point. Different alternatives for defining the DEM parameters via a "local approach" have been reported in recent years [3–5, 12, 16, 21, 22].

In this work we use the local approach for defining the DEM parameters for an arbitrary cohesive material following the procedure explained in [14].

The DEM implementation uses spheres for the representation of the material in 3D. The mesh of spheres is generated trying to minimize the volume of voids. The typical porosity values achieved are about 24%. The particles are considered as rigid, but the contacts between them are visco-elastic [14]. Therefore, the contact happens throughout a range of distances between the particles which can include gaps and penetrations.

The forces at the contact interface between particles are split into normal and tangential forces. The kinematics of the spheres consider displacements and rotations and follow the standard equation of rigid body dynamics. An explicit time integration scheme is used for computing the displacements, velocities and accelerations of each particle, as well as its rotation, angular velocity and acceleration. Appropriate local and global damping parameters are introduced. The material behaviour at the contact interface is considered to be elasto-plastic under compression, with no yield point. Under tension, the material is considered to be linear elastic perfectly brittle. In the tangential direction, the material also exhibits the same linear elastic perfectly brittle behavior with the difference that a residual frictional strength can exist in the presence of normal compressions. Details of the constitutive model are given in [14].

The particular values for the normal and tangential stiffness parameters at the contact interfaces and the limit values of the interface strengths are determined for every material using the local constitutive model described in [14].

3 Setup and modelling of the bottom-hole assembly

The challenge of analyzing and simulating with the DEM a real engineering drilling operation is an extremely complex problem. The use of an optimized geometry and a set of well balanced model parameters is required to keep a reasonably refined discrete element model within the limits of what is feasible with the computational resources available. At the same time, the focus has to be put on the validity and accuracy of the results.

3.1 Drill-bit geometry

A drill bit assembly with casing was taken as the reference model used to recreate the geometry onto which to perform the drilling simulations with the DEM. This tool is designed for drilling-with-casing in medium/hard formations. The characteristic confined compressive strength of such formations can reach up to 130 MPa(15000 psi). The cutters are mounted on the face of the tool to achieve an efficient drilling operation and maximize durability [1]. The drilling tools are modelled with 4-noded linear tetrahedral finite elements. The material properties of standard steel have been chosen for the analysis (Young modulus: 210 GPa, density: 770 $^{kg}/_{m^3}$, Poisson's ratio: $\nu = 0.1$). On the other hand, the soil has been modelled with the DEM using spherical cohesive particles (Figure 1). The particle sizes used are described in Subsection 4.5. Other problem data are given in Subsection 4.3.

Although the real design includes several drilling nozzles to increase the hydraulic power at the bit, these have been removed in the simulation model, along with other detailed design features, in order to reduce the geometric complexity and to improve the computational efficiency.

Specifications	
Nominal size ($in.$)	$7 \times 8 - 1/2$
Number of blades	5
Drilling diameter (in.)	$8 - 1/2$
Tool length (ft)	4.18
Tool weight (lb)	271
Cutter diameter ($in.$)	0.51
Number of face cutters	31
Number of gauge cutters	10

Table 1 Drilling tool specifications

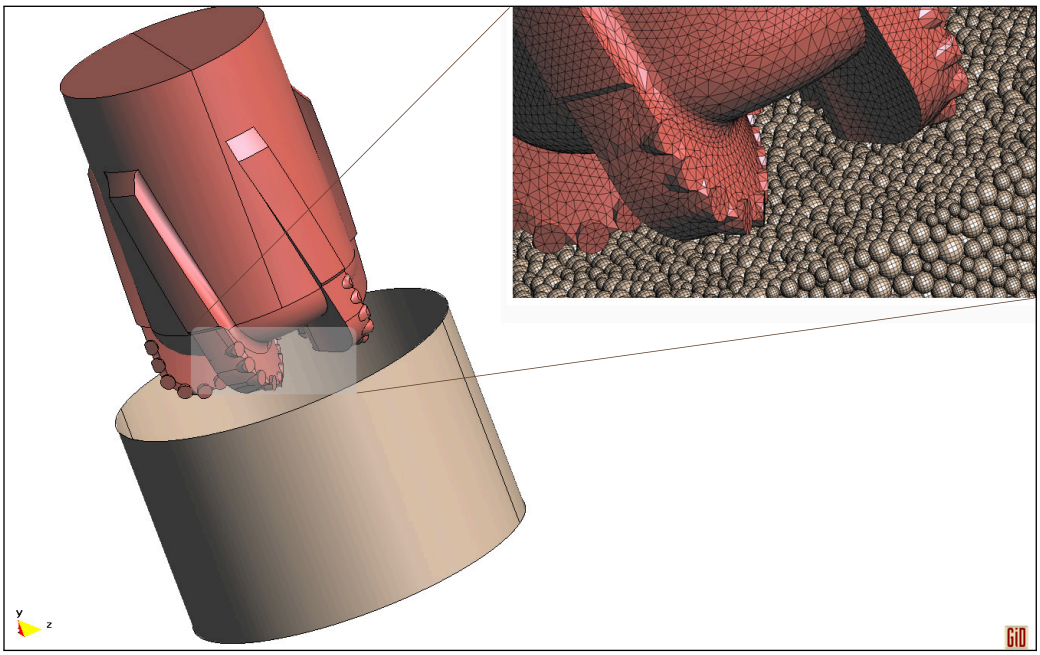

Fig. 1 Initially defined geometry for the drill-bit model. The drilling tools are modelled with 4-noded tetrahedral elements and the soil with spherical particles.

3.2 Soil mechanical properties

The soil material chosen for the drilling simulation was characterized by an unconfined compressive strength of 103 MPa (15000 psi), a limit tensile strength of 10 MPa, a Young's modulus of 345 MPa (50000 psi), a Poisson ratio $\nu = 0.25$, and a density of 2400 $^{\text{kg}}/_{\text{m}^3}$ (0.054 $^{\text{lb}}/_{\text{in}^3}$).

3.3 Operating parameters

Two parameters define the operation of a drill bit: the rotation speed and the vertical force applied on the bit. The rotary speed (RPM) specifications for the polycristalline diamond compact (DPC) bit [1] selected ranges between 60 to 90 RPM. The main simulations were performed with the bit angular velocity Ω set at 80 RPM. A nominal weight-on-bit of 15000 lbf was applied in all the simulations. The drill bit's mass is 58.64 lb although the gravity effect on the tool and particles has not been considered in these simulations.

The key geometrical parameters of the drilling tool are shown in Table 1.

4 Sensibility analysis of the drill bit mechanics

The variability in the output of the simulation model can be due to different sources of uncertainty in its inputs. Because of this, a sensitivity analysis is useful in order to identify model parameters that cause significant variations in the output variables. This sensibility analysis also helps to understand the relationships between input and output variables in the simulated model. At the same time, it allows a subsequent simplification of the study by fixing model inputs that have no effect on the output.

4.1 Effects of the damping factor in the discrete element model

The first parameter analyzed is the damping factor to apply to the soil. By damping factor we understand the coefficient that is applied to the theoretical critical global damping value for the assembled system of

particles ($Damp_{Coef} = \alpha_d \cdot Damp_{Critical}$) [14]. In our work we have considered three different values of the damping coefficient α_d. The observed effect of the particle damping in the drilling simulation is mainly reflected on the decremental values of torque, probably due the modified chip flow around the drill-bit [8, 19] (Figure 2).

Figure 3 shows the influence of the damping factor on the evolution of the axial displacement of the drill tool.

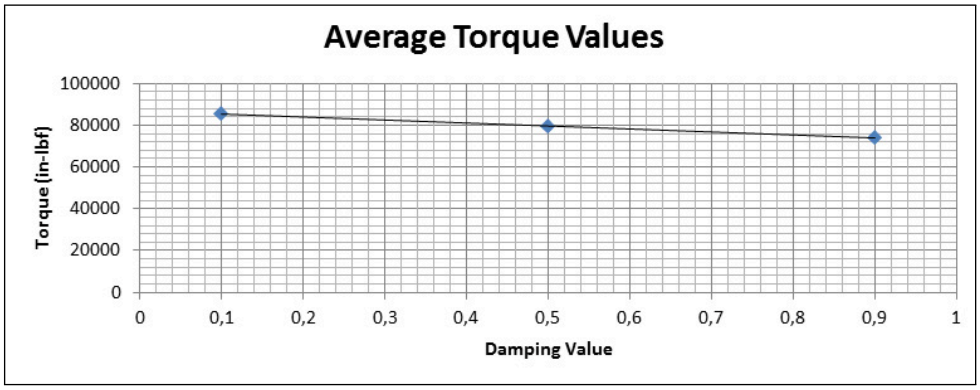

Fig. 2 Torque comparison for each assigned particle damping. Simulations were run using the 12.44 in. geometry model (Figure 5) and 80 rpm.

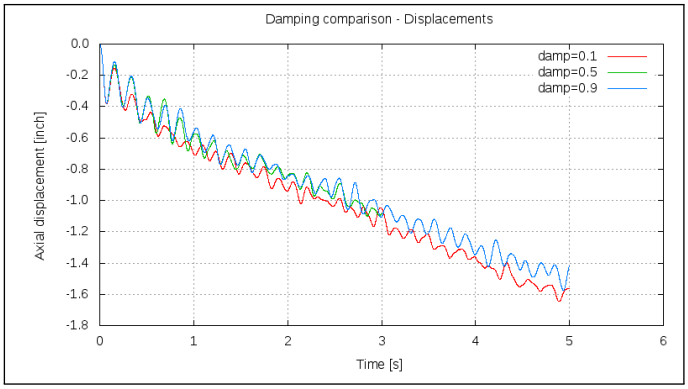

Fig. 3 Axial displacement of the drill tool for each assigned particle damping. Geometry model with 12.44 in. diameter at 80 rpm.

As a result of the small influence observed in the general behavior of the tool, a damping factor of $\alpha_d = 0.9$ was set for the ensuing simulations.

4.2 Influence of the rotational speed

With the damping value already set, simulations for 80 and 100 rpm were run reflecting the penetration rate variation in the obtained velocity and displacement results. Results for the evolution of displacements are depicted in Figure 4. A similar set of results was obtained for the velocity evolution.

No problems were detected while using different rotational speeds of the drill bit, verifying the functionality of the DEM model.

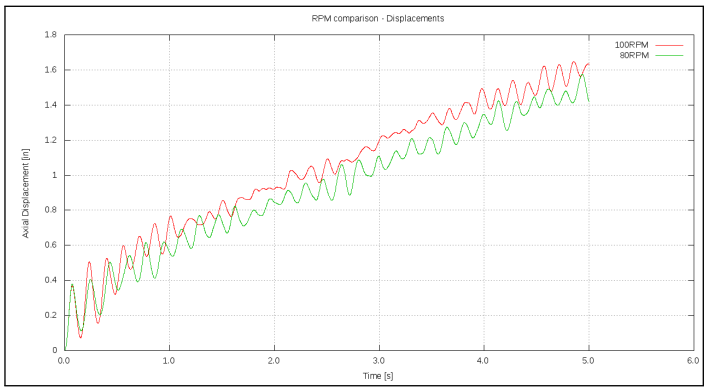

Fig. 4 Displacements comparison for 80 and 100 rpm for the 12.44 in. diameter geometry model. $\alpha_d = 0.9$.

4.3 Soil boundary conditions

The simulations were conducted in different sized soil samples. The purpose of this test was to evaluate the effect of the distance to the boundary on the drilling response. Two sample diameters were simulated: 12.44 in. and 16 in. The total specimen depth was fixed at 7.87 in. For a graphical comparison of the two models see Figure 5. The length of the case surrounding the drill-bit was extended to help controlling the outflow of the flying soil material.

Rigid conditions at the containing boundary surface have been assumed. For this purpose the particles in contact with that surface have been assumed to have zero motion in the normal direction to the boundary. In the tangential directions the motion has been allowed using a simple Coulomb friction model with a friction parameter of $\mu = 0.7$.

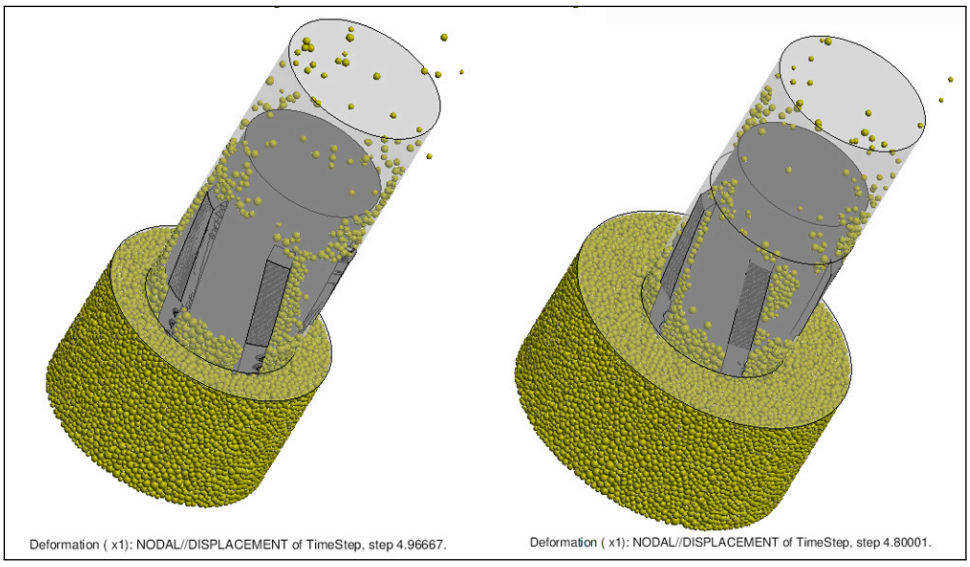

Fig. 5 Analysis geometry for two different soil specimens. Left: $\phi = 12.44$ in. Right: $\phi = 16$ in.

In Table 2 we present a comparison of average torque values and average velocities of penetration for the two samples with tight and loose base geometries with 12.44 in. and 16 in. in diameter, respectively. The difference in velocity results are lesser than 0.5%, while the difference in torque results are of 15%. Given the little variation of these results and provided the computational savings that the smaller geometry provides, we decided to go on with the study using the 12.44 in. diameter sample.

	$\phi = 12.44$ in.	$\phi = 16$ in.
Average Velocity (in/s)	-4.85E-02	-4.87E-02
Average Torque (lbf.in)	1.16E+05	1.01E+05
Test field diameter (in.)	12.44	16
Drill boundary diameter (in.)	9	9
Drilling diameter (in.)	8.5	8.5

Table 2 Average values for each base geometry

4.4 Influence of the time step scale factor

Since the explicit method used for integrating in time the DEM equations of motion is conditionally stable, we aimed to find the biggest possible time step to reduce calculation times. The critical time step (Δt_{cr}) is automatically calculated for a defined mesh and material. In order to optimize the time step (Δt) and based on previous studies [15], four different scale factors were tested $\alpha_t = \{0.10\ , 0.15\ , 0.20\ , 0.25\}$ with

$$\Delta t = \alpha_t \cdot \Delta t_{cr} \tag{1}$$

The graphs in Figure 6 show the average results of torque and rate of penetration for each of the considered values of α_t. Average values were calculated and compared for different times at time intervals of one second.

As shown in the graphs of Figure 7, the frequency peaks for $\alpha_t = \{0.10, 0.15, 0.20\}$ were all consistent and close to 6.5 Hz. Those peaks location changed to 6.2 Hz when using a higher value of $\alpha_t = 0.25$. Finally and according to these evidences, a scale factor of $\alpha_t = 0.20$ was considered acceptable for the model.

This result is in accordance to previous studies in the literature where the value of α_t has been studied by different authors [15] with recommended values close to $\alpha_t = 0.17$ for 3D simulations ($\alpha_t = 0.30$ for the 2D cases).

4.5 Optimum particle size

In the context of the analysis of cohesive material the DEM can be perceived as a discretization method where particles are used to model the mechanics of the underlying continuum. The selection and experimental calibration of an appropriate local constitutive model for representing the particle interaction at the contact interfaces makes the DEM relatively unsensitive to the number of particles [13]. In any case, the number of particles chosen for the analysis affects the computational cost.

The particle size affects the computational cost in two ways. It affects directly by determining the number of spheres used in the discretization of the geometric model. But it also affects indirectly the critical time step according to Eq.(1) and the following relation:

$$\Delta t_{cr} = min\ 2\sqrt{\frac{m_i}{k}} \tag{2}$$

where k is the stiffness of the springs for all the contacts between spheres, and m_i is the mass of particle i. Therefore, assuming that the material density does not vary, the value of Δt_{cr} increases with the particle size.

With the objective to minimize computational times, four models with different particle sizes were tested. Particle sizes of {0.20, 0.22, 0.24, 0.26} inches were used as initial reference when generating the particles (spheres) [9], although the model with 0.20 in. was discarded due its excessive computational cost. Information of the simulation results can be found in Table 3.

The actual average particle size and the number of particles used in each of the simulations can also be found in Table 3. A sample of the particle size distribution for the 0.24 in. mesh is shown in Figure 8. It can be seen that the particle distribution follows a Gaussian function. However, the long tail for small sizes has been trimmed in order to allow for an increase in the critical time step (Δt_{cr}) associated to the model.

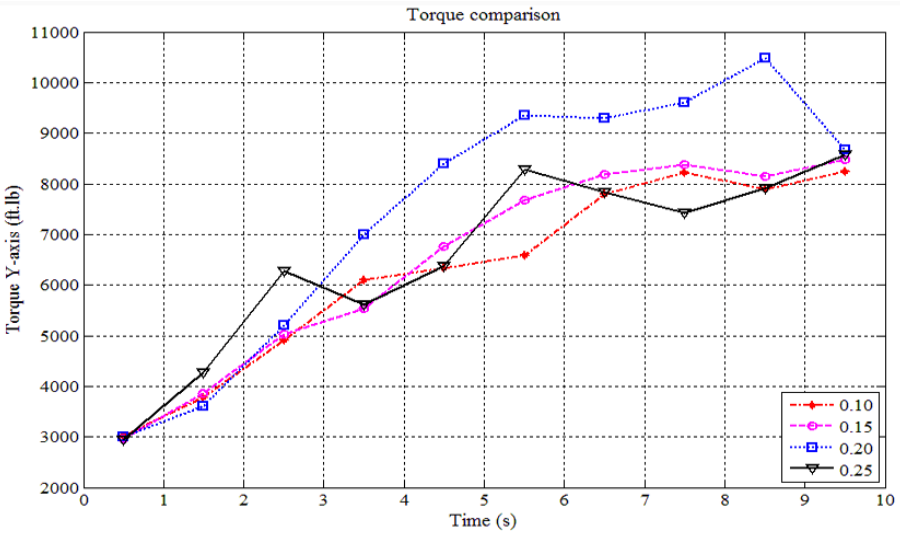

(a) Torque values

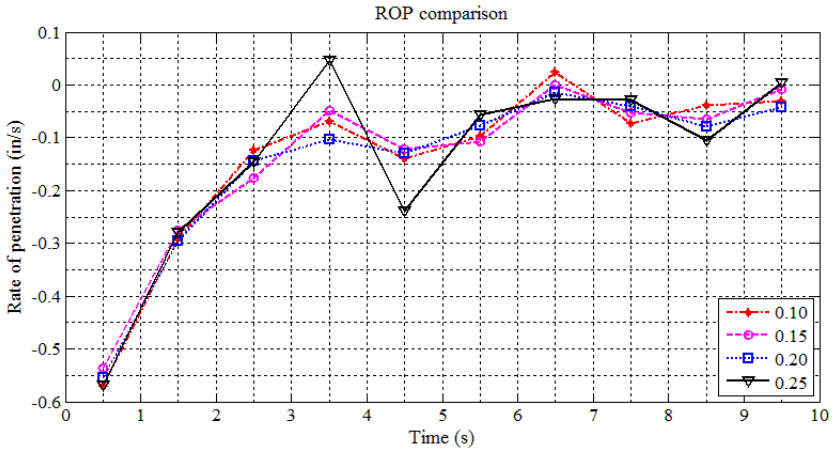

(b) Rate of penetration (ROP)

Fig. 6 Average values of torque and rate of penetration for each α_t factor.

Particle size	Average particle radius (inch)	No of particles	Frequency peaks (Hz)	Amplitude (ft.lb)
0.22 inch	0.141	66000	6.0	480
0.24 inch	0.156	59000	5.9	850
0.26 inch	0.167	54000	6.5	500

Table 3 Torque frequency peaks & wave amplitudes for each reference mesh (15 Hz low-pass filtered data).

Figure 9 shows the comparison of the rate of penetration (ROP) for three of the particle sizes considered in the study. Results have been smoothed with a local regression using a weighted least square method and a second degree polynomial approximation.

A frequency analysis with a fast Fourier transformation (FFT) was done for each of the different particle size models (Figure 10) and similar frequency peak values are observed for the 0.22 in. and 0.24 in. models. The actual values of this study may seem to contrast with the values of the frequency peaks obtained in the study relative to the time step factor α_t, since the mesh size used back in that section was 0.26 in. Also

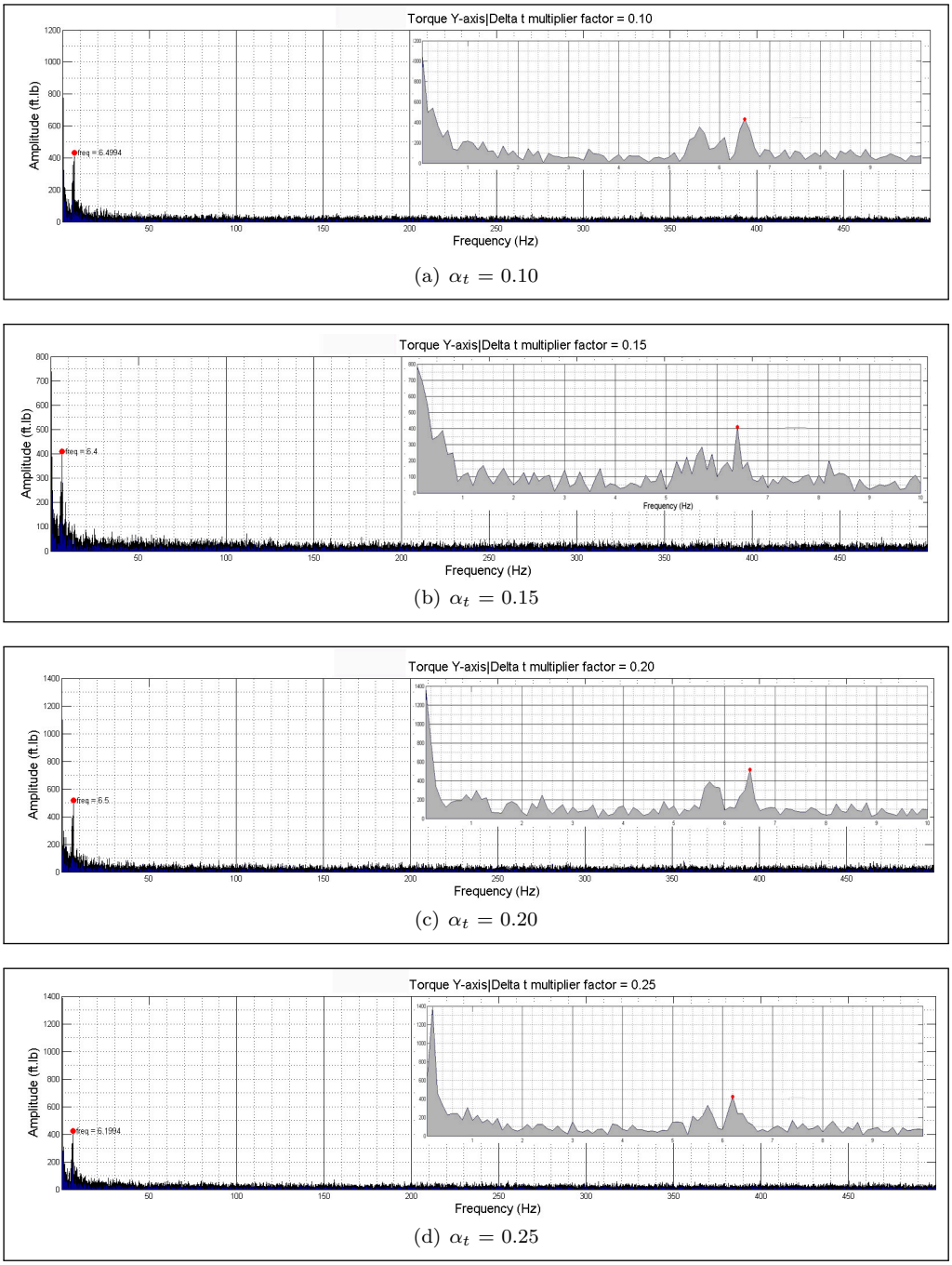

(a) $\alpha_t = 0.10$

(b) $\alpha_t = 0.15$

(c) $\alpha_t = 0.20$

(d) $\alpha_t = 0.25$

Fig. 7 Torque frequency peaks for each α_t factor. Boxes show a detail of the peaks for the low frequencies range.

a 15 Hz low-pass FFT filter was applied to the torque-time diagram for each generated mesh (Figure 11) in which simulations for both $r_1 = 0.22$ in. and $r_2 = 0.24$ in. yielded similar results. This is consistent with the observation above, thus suggesting that an average particle radius of $r_2 = 0.24$ in. will provide an adequate accuracy with the least computational cost.

Based on all these results, the mesh generated with a reference average size of the spheres of 0.24 in. was chosen for the subsequent tests. This mesh yielded similar results both in magnitude and frequency peak to

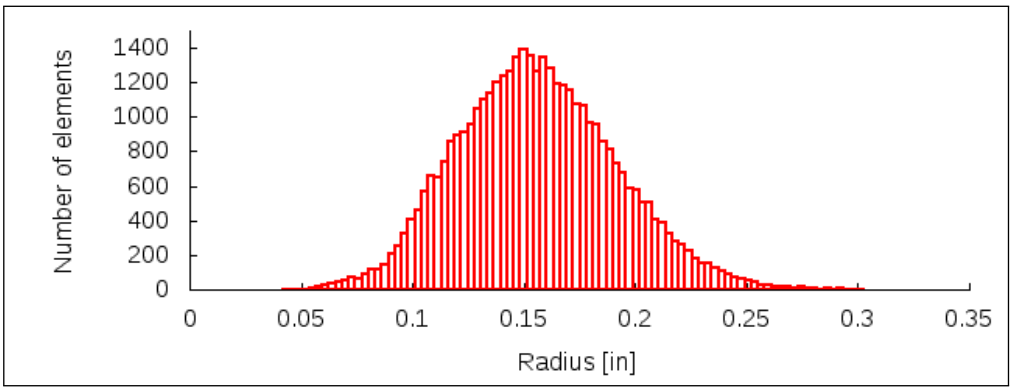

Fig. 8 Mesh quality of the 12.44 in. diameter geometry model shown as the distribution of radius sizes of the spheres in the mesh.

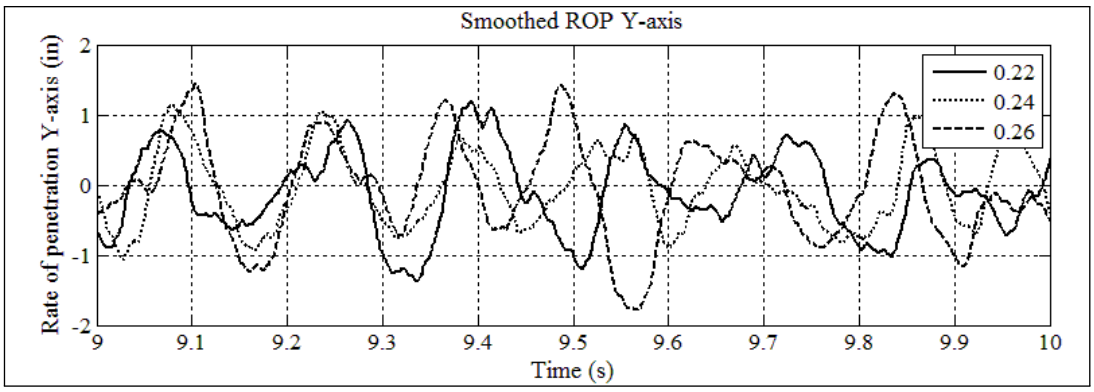

Fig. 9 Rate of penetration (ROP) comparison smoothed with a local regression using weighted linear least squares and a 2nd degree polynomial model.

those of the mesh with a reference average size of 0.22 in. On the other hand, the 0.26 in. mesh size results differed both in magnitude and peak frequency.

4.6 Steady state

Having studied the main model parameters that could potentially affect the performance of the model, several preliminary outputs were obtained from the initial simulations. One key issue in the modelling of a bottom-hole assembly (BHA) and its response while under load is being able to ensure that some conditions are met. In particular, the steady state condition must be achieved.

It is estimated that the steady state will be attained (i.e. the effect of the initial conditions is can be disregarded) when the full length of the cutting blades are buried into the soil material (see Figure 12). For this reason we decided to increase the simulation time from the initial 10 seconds to 40 seconds. With this extension we estimated that the depth of the drill would reach the 10 in. needed to bury the blades in the soil sample. The results are illustrated in the depth-time diagram shown in Figure 13. The drilling response beyond the 10 s threshold confirmed additional simulation time was absolutely required in order to achieve a steady behavior. In fact, the rate of penetration slows considerably as the flat bottom of the drilling tool reaches the sample (Figure 14). Note that after 40 seconds of simulation, only 3 in. of penetration are achieved. This is in contrast with the 10 in. we were looking for. The evolution from the transient state to the steady state ($t > 40$s) can also be observed in the torque results (Figure 15).

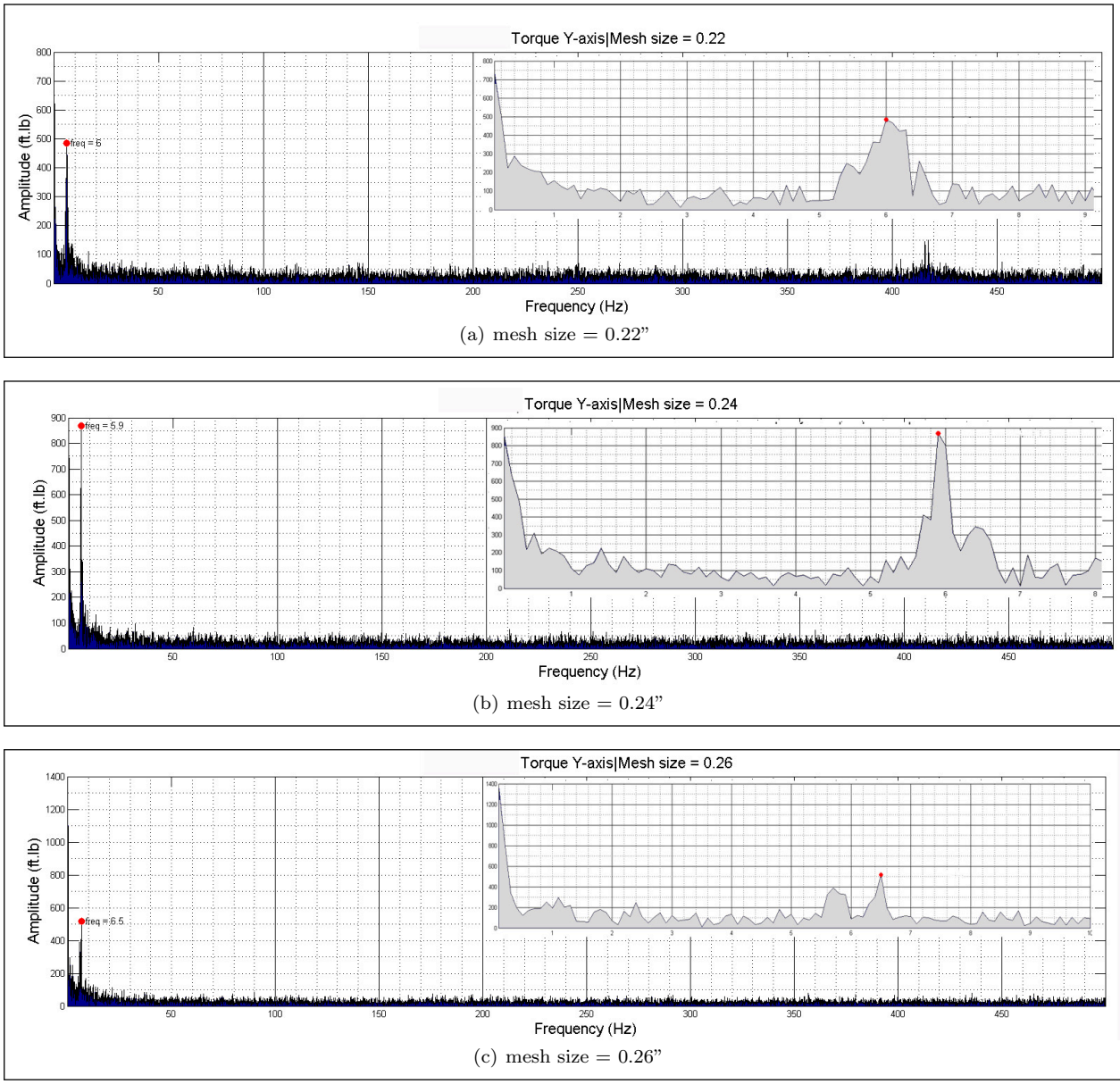

(a) mesh size = 0.22"

(b) mesh size = 0.24"

(c) mesh size = 0.26"

Fig. 10 Torque frequency peaks for each reference mesh size.

5 Conclusions

Results obtained in the study of the drill-bit region using the DEM indicate that this method is applicable to study the mechanical performance of oil and gas drilling operations. The information provided by the method is richer than the existing semi-empirical models. However, further validation of the method with a wide range of soils and geological formations is required. The model presented here reproduces well the behavior of the soil as a linear elastic and perfectly brittle material. The local DEM model used has algo demonstrated a good behaviours for other geomaterials that show a more ductile behaviour. This is a promising result for future applications of the DEM in the oil and gas drilling industry.

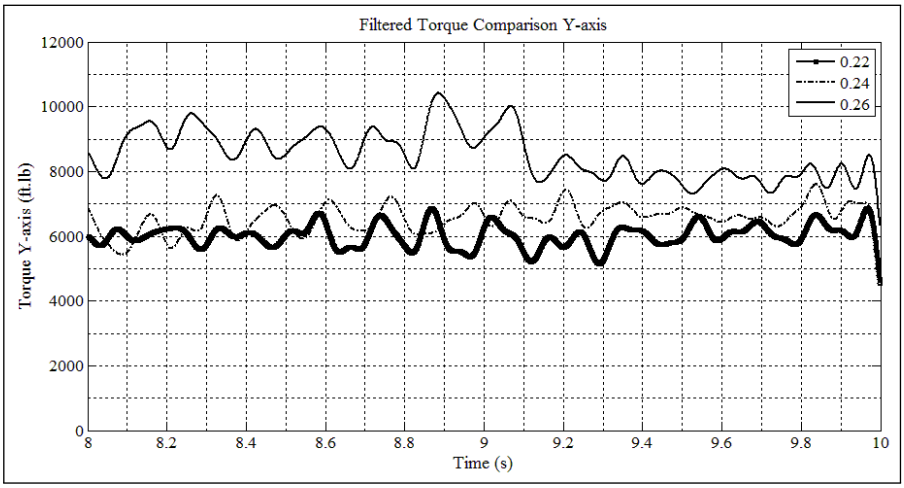

Fig. 11 15 Hz low-pass FFT filtered torque comparison for each reference mesh size.

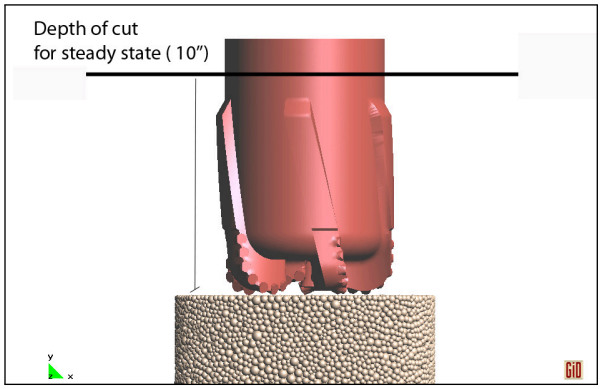

Fig. 12 Considered steady state depth of cut.

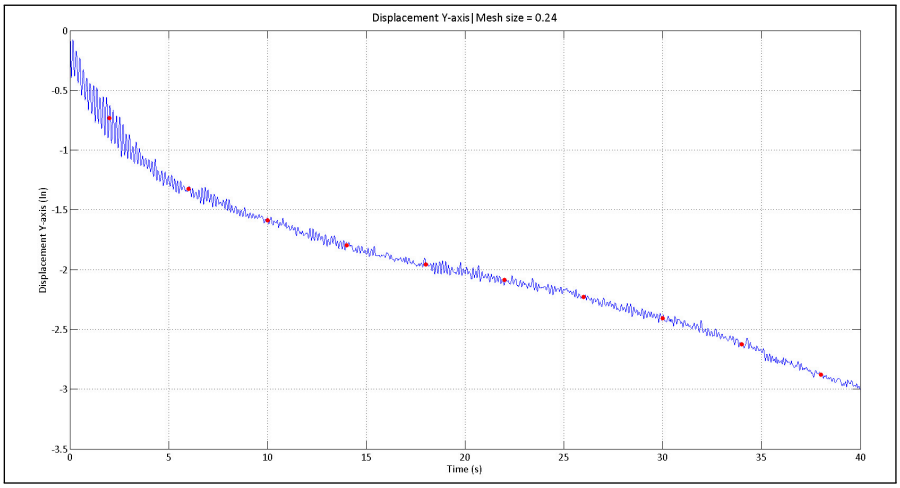

Fig. 13 Vertical displacement of the drill bit for the first 40 seconds of simulation. Average ROP for $t = [10\,\text{s}–40\,\text{s}]$ is $v = -0.046\,\text{in/s}$

Another line of improvement will be the acceleration of the simulation software through the use of parallel computers and the development of advanced numerical techniques. These include: enhanced contact search algorithms and fast database management, besides enhanced and robust numerical solvers.

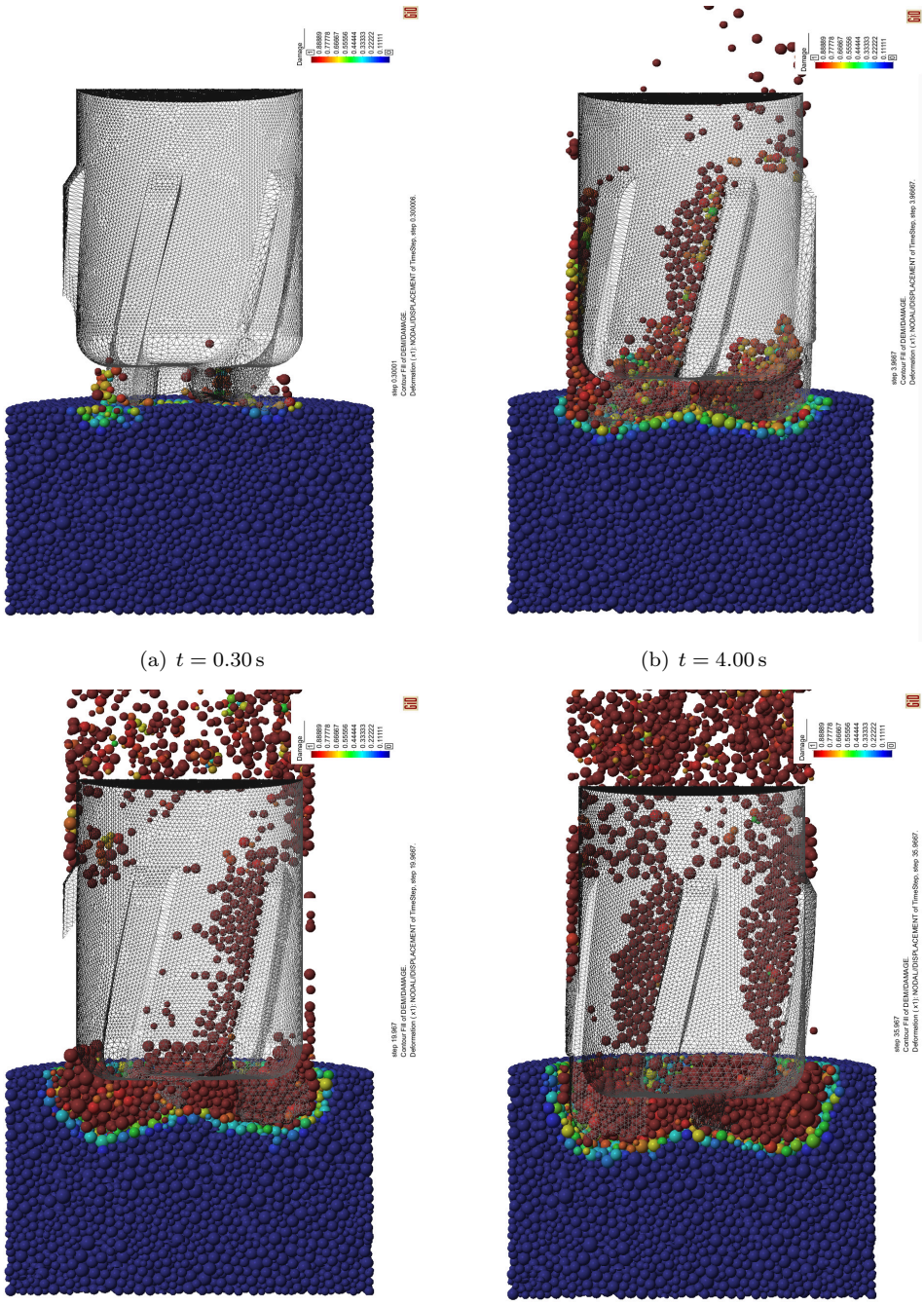

(a) $t = 0.30\,\mathrm{s}$ (b) $t = 4.00\,\mathrm{s}$

(c) $t = 20.00\,\mathrm{s}$ (d) $t = 36.00\,\mathrm{s}$

Fig. 14 Visualization of the drilling process evolution in the drill-bit region using a longitudinal cut of the soil sample. The colors represent the damage of the soil particles (i.e. the number of broken bonds).

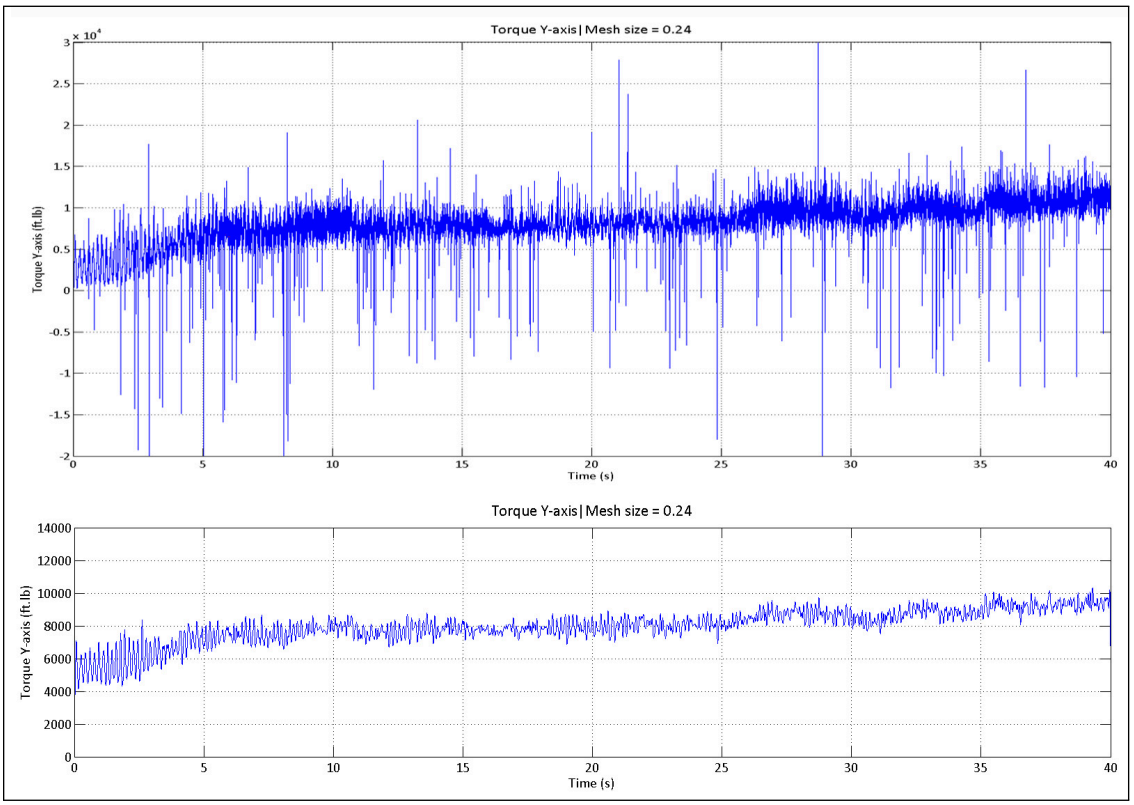

Fig. 15 Evolution of the torque reactions for the model using a soil sample of 0.24 in. diameter. The upper graph shows the unfiltered data. The lower graph shows the same data after applying a 15 Hz low pass filter. Steady-state conditions are assumed to occur at $t > 40$s

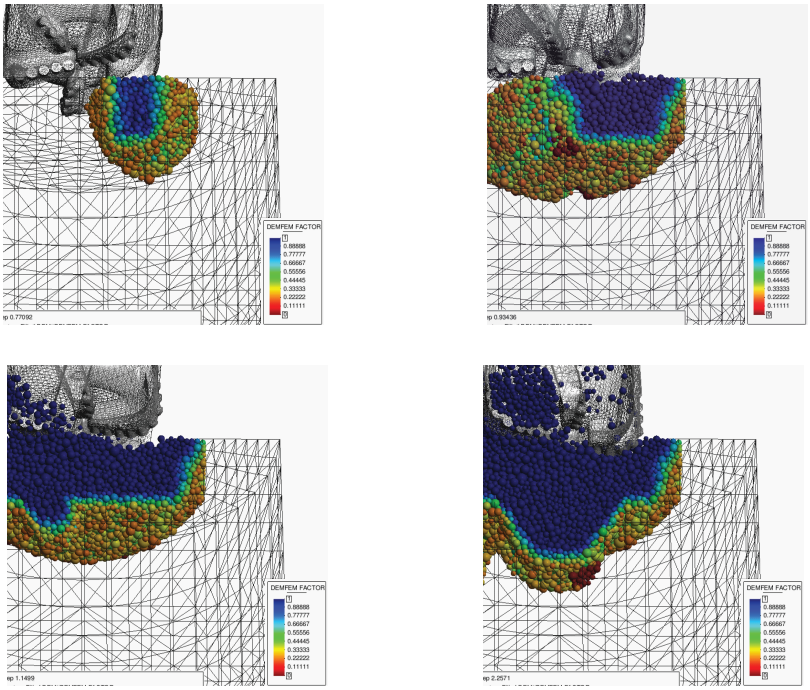

Fig. 16 Drilling process modelled with an adaptive FEM-DEM technique

A very promising technique to reduce the required computational times is to combine the FEM with the DEM for modelling the multifracture in the soil in the drill-bit region. The idea is to model the intacted soil region with the FEM and to introduce the DEM in the fractured zone in an adaptive and progressive manner. Examples of this FEM-DEM approach have been reported by the authors [13]. As an example, Figure 16 shows the evolution of the cutting tool in a soil mass initially modelled with the FEM using 4-noded tetrahedra. DEM particles are progressively created in the drill tip region as the stress level increases in this area. The FEM-DEM approach has the advantage of reducing the number of degrees of freedom of the overall model and thus decreasing the computational time needed to run the simulations. [12, 13, 23].

Drilling systems permanently experience torsional vibrations. One feature of the long drill string system is its torsional elasticity, which combined with the dynamics of the drilling mechanics can produce the undesired stick-slip phenomenon. Stick-slip events are an important cause for drillstring failures and drill bit breakages. The implementation of a 3D beam element able to reproduce the behavior of a drillstring in a rotary drilling system will allow us studying the motion responsible for self-excited vibrations, and its effect on the delivered torque and weight-on-bit [2].

6 Acknowledgements

Financial support for this work was provided by Weatherford. The authors thank Dr. C. Labra for many useful discussions.

The numerical results presented in this work have been obtained with the code DEMPACK developed at CIMNE (www.cimne.com/dempack).

REFERENCES

1. Defyer DPC Series. Weatherford International Ltd., 515 Post Oak Blvd. Houston, Texas, 2005. 4674.02.
2. J.M. Carbonell, N. Abedrabbo, M.A. Celigueta and E. Oñate. A 3D beam element for analysis of the drill string mechanics in boreholes. Research Report CIMNE, PI411, Barcelona, October 2015.
3. F. Donzé, F. Richefeu and S. Magnier. Advances in discrete element method applied to soil, rock and concrete mechanics. *Electronic Journal of Geotechology Engineering* 08, 144, Special volume, Bouquet, 2009.
4. A. Fakhimi and T. Villegas. Application of dimensional analysis in calibration of a discrete element model for rock deformation and fracture. *Rock Mechanics and Rock Engineering*, 40(2):193–211, 2007.
5. S. Hentz, L. Daudeville and F. Donzé. Identification and validation of a discrete element model for concrete. J. of Engineering Mechanics, 130(6):709–719, 2004.
6. Y.-M. Hsieh, H.-H. Li, T.-H. Huang and F.-S. Jeng. Interpretations on how the macroscopic mechanical behavior of sandstone affected by microscopic properties revealed by bonded-particle model. *Engineering Geology*, 110, 2008.
7. H. Huang. *Discrete element modeling of tool-rock interaction*. Ph.D. Thesis, December, University of Minnesota, 1999.
8. C. Labra, J. Rojek, E. Oñate, and F. Zarate. Advances in discrete element modeling of underground excavations. *Acta Geotechnica*, 3:317–322, 2008.
9. C. Labra and E. Oñate. High-density sphere packing for discrete element method simulations. *Communications in Numerical Methods in Engineering*, 25(7):837–849, 2009.
10. C. Labra, J. Rojek, E. Oñate and F. Zárate. Advances in discrete element modelling of underground excavati ons. *Acta Geotechnica*, 3(4):317–322, 2009.
11. C. Labra. *Advances in the development of the discrete element method for excavation processes*. Ph.D. Thesis. Technical University of Catalonia, UPC, July 2012.
12. E. Oñate and J. Rojek. Combination of discrete element and finite element methods for dynamic analysis of geomechanics problems. *Comput. Meth. Appl. Mech. Engrg.*, 193:3087–3128, 2004.
13. E. Oñate, C. Labra, F. Zárate, and J. Rojek. Modelling and simulation of the effect of blest loading an structure using an adaptive blending of discrete and finite element method. 3rd International Week

on Risk Analysis, Dam Safety, Dam Secutiry and Critical Infraestructure Management. Valencia, Spain, 17–18 October 2011.
14. E. Oñate, F. Zárate, J. Miquel, M. Santasusana, M.A. Celigueta, F. Arrufat, R. Gandikota, Khardar and L. Ring. A local constitutive model for the discrete element method. application to geomaterials and concrete. Comput. Particle Mech., 2(2):139–160, 2015.
15. C. O'Sullivan and J. Bray. Selecting a suitable time step for discrete element simulations that use the central difference time integration scheme. *Engineering Computations*, 21:278–303, 2004.
16. D. Potyondy and P. Cundall. A bonded-particle model for rock. *International Journal of Rock Mechanics and Mining Sciences*, 41(8):13291364, Rock Mechanics Results from the Underground Research Laboratory, Canada, 2004.
17. J. Rojek, E. Oñate and F. Zarate, and J. Miquel. Modelling of rock, soil and granular materials using spherical elements. In *2nd European Conference on Computational Mechanics ECCM-2001*, Cracow, 26-29 June, 2001.
18. J. Rojek and E. Oñate. Multiscale analysis using a coupled discrete/finite element model. *Interaction and Multiscale Mechanics*, 1(1):1–31, 2007.
19. J. Rojek, E. Oñate, H. Kargl, C. Labra, J. Akerman, U. Restener, E. Lammer, and F. Zarate. Prediction of wear of roadheader picks using numerical simulations. *Geomechanik und Tunnelbau*, 1:47–54, 2008.
20. J. Rojek, C. Labra, O. Su and E. Oñate. Comparative study of different micromechanical parameters. *Int. J. of Solids and Structures*, 49:1497–1517, 2012.
21. F.A. Tavarez and M.E. Plesha. Discrete element method for modelling solid and particulate materials. *International Journal for Numerical Methods in Engineering*, 70(4):379–404, 2007.
22. V.T. Tran, F.-V. Donzé and P. Marin. A discrete element model of concrete under high triaxial loading. *Cement & Concrete Composites*, 33:936–948, 2011.
23. F. Zárate and E. Oñate. A simple FEM-DEM technique for fracture prediction in materials and structures. Submitted to *Computational Particle Mechanics*, DOI: 10.1007/s40571-015-0067-2, 2015.